Inorganic Chemistry

Article

pubs.acs.org/IC

π-Rich σ^2P-Heterocycles: Bent η^1-P- and μ^2-P-Coordinated 1,3-Benzazaphosphole Copper(I) Halide Complexes

Mohammed Ghalib,[†,⊥] Peter G. Jones,[‡] Carola Schulzke,[§] Dénes Sziebert,[∥] László Nyulászi,*[,∥] and Joachim W. Heinicke*[,†]

[†]Institut für Biochemie – Anorganische Chemie, EMA-Universität Greifswald, 17487 Greifswald, Germany

[‡]Institut für Anorganische u. Analytische Chemie, Technische Universität Braunschweig, 38106 Braunschweig, Germany

[§]Institut für Biochemie – Bioanorganische Chemie, EMA-Universität Greifswald, 17487 Greifswald, Germany

[∥]Department of Inorganic and Analytical Chemistry, Budapest University of Technology and Economics, H-1521 Budapest, Hungary

Supporting Information

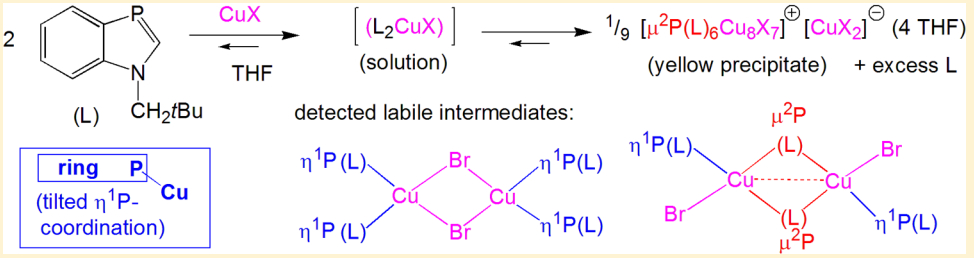

ABSTRACT: The reaction of 1-neopentyl-1,3-benzazaphosphole **1** with CuCl, CuBr, or Cu(SMe$_2$)Br in THF at room temperature provides sparingly soluble $[Cu_7(\mu^2\text{-}L_6)(\mu^2\text{-}X_7)]^+[CuX_2]^-$ cluster complexes **2a**,**b** (L indicates coordinated **1**, **a** X = Cl, **b** X = Br), with loosely bound THF, in high yields. The conversions proceed via transient THF-soluble labile $[(L_2CuX)_2]$ complexes. Separation before complete conversion, combined with suitable conditions for crystallization, allowed these intermediates to be trapped. Depending on the reactant ratios, crystals of the clusters or of dimeric L_2CuX complexes were formed. The crystal structure analyses of **2a**·4THF and the dimers **3b** $[\{Cu(\eta^1\text{-}L)_2(\mu^2\text{-}Br)\}_2]$, **4b** $[\{Cu(\mu^2\text{-}L)(\eta^1\text{-}L)(\kappa Br)\}_2]$, **5a**·2MeOH, and **5b**·2MeOH $[\{Cu(\mu^2\text{-}L)(\eta^1\text{-}L)(\kappa X\cdots HOMe)\}_2]$ generally display μ^2-P- and/or tilted η^1-P-coordination, contrasting with the preference for the η^1-P in-plane coordination mode of phosphinine ligands in their copper(I) halide complexes. DFT studies of geometry-optimized monomers LCuBr, $L(CuBr)_2$, L_2CuBr, and the dimers **3b** and **4b**, calculated at the ωB97xD/cc-PVDZ level, suggest that weak competing interactions with the solvent THF and the entropy factor of the dimerization result in lability and a subtle balance between the different complexes in solution, whereas the particular coordination observed in the crystals is attributable to conservation of the delocalized π-system in the ligand. The HOMO of **4b** is composed of Cu d orbitals and the π-type HOMO of the bridging ligand. Interestingly, despite the rather short Cu···Cu interatomic separation (2.726 Å), no bond critical point could be located in **4b**, indicating the absence of weak cuprophilic interactions in this compound.

INTRODUCTION

Compounds of trivalent phosphorus are well established as widely tunable ligands in coordination chemistry and homogeneous transition metal catalysis.[1,2] In comparison with systems of σ^3P-ligands, however, transition metal complexes and catalysts with dicoordinated (σ^2P) phosphorus ligands have been much less thoroughly investigated, and most of these studies concern phosphabenzene (phosphinine)[3] or phosphaalkene[4] ligands. For π-excess-aromatic neutral 1*H*-1,3-azaphosphole ligands, a variety of metal(0) complexes is known,[5,6] stabilized by π-back bonding as is typical in the case of σ^2P-ligands, but complexes with nonzero-valent metals are extremely rare. Only a few η^1-P- or N-coordinated di- and triazaphosphole Me_2AuCl, $PtCl_2$, and ReBr-complexes,[7] an N,N-bridged bis-(1,2,3-cyclohexenodiazaphosphole)$HgCl_2$ cluster[8] and a single carbocyclic annulated (1,2-azaphosphole)allylnickel chloride complex[9] have been published by other groups; we have recently reported the first *1H*-1,3-benzazaphosphole AgX (X = Cl, SbF_6) and $HgCl_2$ complexes and a tetranuclear CuOac complex with two μ^2-P benzazaphosphole bridges, stabilizing a butterfly folded tetrameric copper(I) acetate in a distorted tetrahedral arrangement.[10] We now wished to find out whether the peculiar μ^2-P bridging and tilted η^1-P coordination, not observed in the other mono-, di-, and triazaphosphole complexes and rarely even in the more widely explored phosphinine complexes, is a general feature of d^{10} metal complexes of more π-electron-rich 1,3-azaphosphole ligands with the π-donor N atom in conjugation to the low-coordinated phosphorus.We have therefore extended our investigations to novel di- and multinuclear benzazaphosphole copper(I) halide complexes.

Received: September 28, 2014
Published: February 9, 2015

DOI: 10.1021/ic502367d
Inorg. Chem. 2015, 54, 2117–2127

Scheme 1. Structurally Characterized Compounds Formed by Reaction of 1 with CuX (a X = Cl, b X = Br) or Cu(SMe$_2$)Br (L = coordinated 1) in THF; Reactant Ratios of 1:CuX Were Varied According to x:y = 2:1, 1:1, 1:2, and 1:3

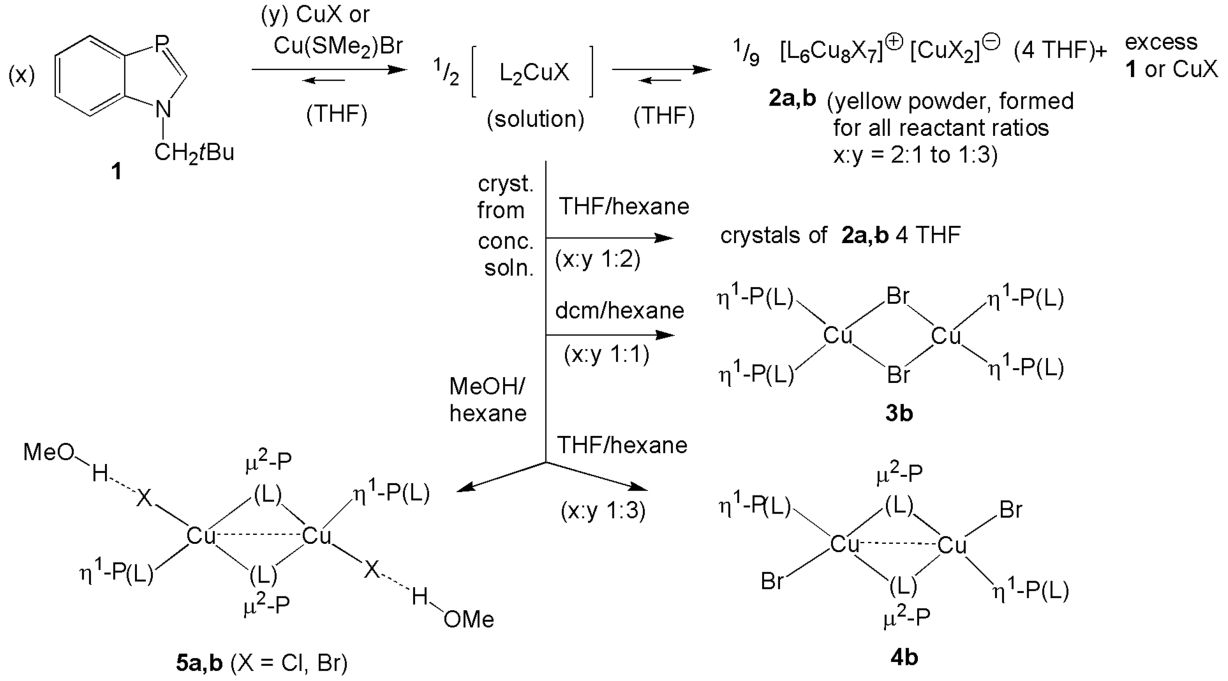

RESULTS AND DISCUSSION

Complex Formation. 1-Neopentyl-1,3-benzazaphosphole (**1**)[11] was chosen as model ligand. It is available in good yield and is suitable for reaction monitoring by NMR. Furthermore, it has been characterized by its crystal structure, thus allowing recognition of structural changes upon coordination. The reactions of **1** with varying amounts of CuCl, CuBr, or Cu(SMe$_2$)Br (Scheme 1) were carried out in THF, by addition of the solvent to the mixtures of solid **1** and the copper halide at room temperature (ca. 22 °C). This resulted generally in an immediate color change to yellow, indicating incipient coordination of dissolved **1** to the copper halide, and in the formation of suspensions. Reaction of **1** and CuX (X = Cl, Br) in a reactant ratio of 2:1 led to almost complete conversion of CuX. The reaction time varied with the crystallinity of the copper halides from less than 1 day to ca. 4 days. The elemental analyses of the resulting yellow solids, worked up by filtration, washing with THF and drying under vacuum, displayed CHN values in agreement with the formation of the clusters **2a** (X = Cl) and **2b** (X = Br), composed of **1** and CuX in the molar ratio 2:3. The THF, loosely bound at the clusters, was removed more or less completely during drying under vacuum and slight warming or after prolonged storage. Samples that were dried for a short time at room temperature contained up to 2/3 THF per coordinated ligand, based on ^{1}H NMR integration of NCH$_2$ and OCH$_2$ signals. Similar yellow solids were formed under the same conditions from **1** and CuX in a reactant ratio of 1:1, and their analyses also indicated the formation of **2a,b**, in this case with small amounts of residual THF (determined from analytical H/N ratios) and unconverted CuX; the solids prepared with reactant ratios of 1:2 or 1:3 of **1** and CuX were mixtures of **2a,b** with larger amounts of unconverted CuX. Removal of the solvent from the filtrates left pale yellow viscous residues, containing minor amounts of labile L$_n$CuX complexes (n = 2 in identified dimer intermediates) and/or unidentified phosphorus compounds. In the case of 2:1 reactant ratios, uncoordinated **1** was recovered in crystalline form from concentrated MeOH solutions of the THF soluble part of the reaction mixture, although the solution ^{31}P NMR spectra displayed signals of weakly coordinated ligand (δ = 65 (at CuCl), 68 (at CuBr) versus δ = 71 for **1**). If the reaction time was insufficient for complete conversion, the amounts of unconverted CuX in the yellow solids were larger, as were the amounts of the viscous products obtained on evaporation of the solvent from the filtrates. Slow diffusion of hexane into the concentrated solutions of these viscous products in either THF or methanol and residual THF led, depending on the ligand to CuX ratio and the absence or presence of MeOH, to solubility-driven formation of crystals of **2a,b**·4THF or dimeric bis(benzazaphosphole) Cu(I) halide complexes **3b**, **4b**, **4b′**, **5a**·2MeOH, and **5b**·2MeOH (Scheme 1). Reactions of **1** with CuBr in CD$_2$Cl$_2$ proceeded similarly to those in THF and provided a yellow solid via soluble intermediates (see below). Use of the μ^2S-bridged Cu(SMe$_2$)Br[12] led to fast initial formation of yellow solutions, followed by slow precipitation of yellow solids. Elemental analyses of the vacuum-dried powders hint in this case at a composition L$_6$(CuBr)$_8$ **2b#**, but suitable crystals to determine whether the structure is related to that of **2b**, but containing Br$^-$ instead of [CuBr$_2$]$^-$, could not be obtained. Incomplete conversion allowed the isolation of single crystals of **3b** by slow evaporation of solvent from a CD$_2$Cl$_2$ solution of the filtrate. They were identical to those obtained from **1** and CuBr.

Structural Aspects. The presence of benzazaphosphole complexes was unambiguously demonstrated by the ^{1}H and ^{13}C solution NMR spectra of both the yellow solids and the compounds in the filtrates (Figures S1−S6). The former are insoluble in the reaction medium THF and also in CDCl$_3$, CD$_2$Cl$_2$, C$_6$D$_6$, CD$_3$OD, or D$_6$-acetone. In D$_6$-DMSO, however, they are reasonably soluble. Most of the proton and ^{13}C NMR signals of the coordinated ligands are sharp and affected only slightly by the coordination. This holds also for the strong

DOI: 10.1021/ic502367d
Inorg. Chem. 2015, 54, 2117−2127

downfield position of the NCH_2 proton signals at $\delta \approx 4.2$. This is attributable to a ring current effect and indicates that the aromaticity of the ligand[13] is not noticeably weakened by the coordination of Cu(I). Only the CH-2, C_q-3a, and CH-4 nuclei, close to phosphorus and the coordinated copper, exhibit changes, broadened signals or reduced P-C and P-H coupling constants, and in **2a,b** significant ^{13}C upfield coordination chemical shifts of the C-2 and C_q-3a nuclei. In contrast to the ^1H and ^{13}C NMR signals, the ^{31}P resonances of the complexes are usually broad and sensitive to even relatively small variations in the ligand/CuX ratio. The complexes **2a** and **2b**, formed from **1** and the corresponding copper halide with reactant ratios 2:1, each display at room temperature one phosphorus signal in this solvent, at δ = 35.9 and 32.9, respectively, with half widths of 15−20 Hz. This corresponds to upfield coordination chemical shifts of $\Delta\delta$ = −35 and −38. The yellow complex formed with $Cu(SMe_2)Br$ (molar ratio 1:1) in THF displayed the ^{31}P resonances at δ = 43 and thus with lower upfield coordination shift. In contrast, samples of **2a** and **2b**, containing unconverted CuX after preparation with excess copper halide, reveal broader (half widths of 30−80 Hz) phosphorus resonances shifted farther upfield, increasing with increasing content of CuX. This implies that the complexes dissolved in DMSO, including those derived from excess CuX, are labile at room temperature and undergo ligand exchange reactions within the NMR time scale, leading to averaged signals. Because no single crystals for unambiguous structure determination were obtained, the true nature of the complexes in DMSO and their interactions with the solvent remains unclear.

The room temperature ^{31}P NMR spectra of the soluble compounds in the filtrate fractions, separated before complete conversion to **2a** or **2b** and measured in CD_3OD, $CDCl_3$, or CD_2Cl_2, likewise indicate labile complexes. The phosphorus signals are averaged in the range $\delta \approx 65$ to 51, corresponding to $\Delta\delta \approx -6$ to −20, respectively, and line widths vary from 25 to 90 Hz. The smaller upfield coordination shifts compared to those of the solutions of **2a,b** indicate higher ligand to copper ratios. VT-NMR measurements of soluble complexes, prepared directly from **1** and CuBr (molar ratio 1:1) in CD_2Cl_2 and separated from the precipitate after 1.5 h, indicated strong line broadening on cooling from 25 to −72 °C, in the proton spectra particularly for the signals of H2 and H4 close to phosphorus (Figure S7, Supporting Information). Additional signals were not observed. In the ^{31}P NMR spectra (Figure S8), the line broadening (half-width at 25 °C 16 Hz, at −72 °C 810 Hz) was connected with a slight upfield shift from δ = 59.3 at 25 °C to $\delta \approx 55$ at −22 and −46 °C. At −72 °C, the major signal was further broadened but again downfield shifted ($\delta \approx 59$) and accompanied by less intense broad signals at $\delta \approx 53$, 43−41, and −6. Warming to room temperature reproduced the original spectra and gave evidence of the reversibility of the changes. The nature of the processes that cause the temperature-dependent alterations could not be derived from the NMR data. The dynamic behavior suggests, however, that the complexes can adopt energetically similar structures that may interconvert with low activation barriers.

More detailed information on the structures of the benzazaphosphole copper halide complexes was gained from X-ray analyses of suitable crystals of **2a**·4THF and the [(L$_2$CuX)2] complexes **3b**, **4b**, **4b′**, **5a**·2MeOH, and **5b**·2MeOH, selected from the mixtures with mother liquor. The crystals of **2a** and **2b**, grown from the filtrate of the 1:2 reaction, tend to disorder of the loosely bound THF and the anion. For **2b**, a very imprecise structure indicated the presence of cationic $[L_6Cu_8Br_7]^+$. For **2a**, a full structure analysis was possible, though some disorder limited the precision. This compound, crystallizing in the triclinic space group $P\bar{1}$ with four molecules per unit cell, is composed of the cation $[L_6Cu_8Cl_7]^+$, the anion $[CuCl_2]^-$ and four THF molecules (Figure 1) and represents to

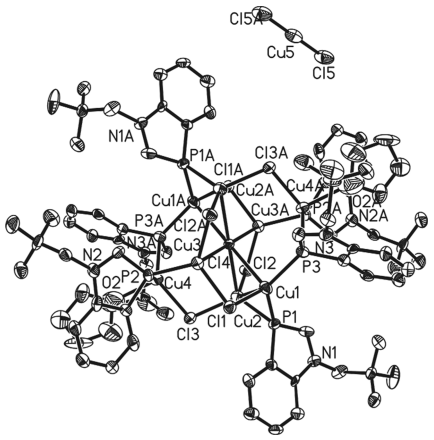

Figure 1. Structure of **2a**·4THF in the crystal (hydrogen atoms and solvent molecules omitted for clarity, ellipsoids with 50% probability). Selected bond lengths (Å) and angles (°): Cu−P 2.229(3) (Cu3−P2) to 2.345(4) (C4_a-P2), Cu−Cl(1−3) 2.241(3) (Cu4_a-Cl3) to 2.296(3) (Cu3−Cl1), Cu−Cl4 2.710(2) (Cu2−Cl4) to 2.759(2) (Cu3−Cl4), Cu···Cu μP-bridged 2.909 (Cu1−P1−Cu2) to 3.785 (Cu1−P3−Cu4A), Cu···Cu μCl-bridged 3.215 (Cu1−Cl1−Cu3) to 3.651 (Cu2−Cl3−Cu4); for further data see Table 1.

the best of our knowledge an unprecedented cluster type with σ^2-P ligands.

The Cu_8-cluster (Figure 2) is build up from two eight-membered ellipsoidal rings forming a crown (in Figure 2 right

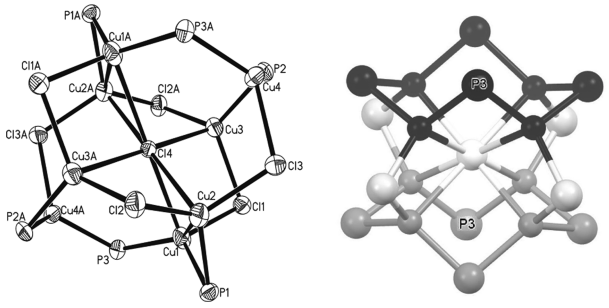

Figure 2. Structure of the $L_6Cu_8Br_7$ cluster cation of **2a**·4THF (Cu4 and Cu4A are disordered; the major components are depicted on the left; the lesser components on the right are presented in gray scale spheres to better visualize the eight-membered crowns at the top and bottom; data in the text referring to the weaker occupied positions are indicated by Cu4_b or Cu4A−b; μ^2-P ligands are represented by the P-atoms).

depicted in black and gray). In each ring four Cu atoms (Cu1A, Cu3A, Cu2, Cu4 at the top, Cu1, Cu3, Cu2A, Cu4A at the bottom) form the base and are bridged by three μ^2-Cl and one μ^2-P ligand (P3A, P3) forming the tips of the crown. Cl4 (shown in white in Figure 2) occupies a local, noncrystallographic inversion center, which is particularly relevant regarding P3 and P3A, and bridges six to eight (depending on which component of the disordered Cu4 is taken into account) Cu

DOI: 10.1021/ic502367d
Inorg. Chem. 2015, 54, 2117−2127

atoms (2.710(2) to 2.759(2) Å). The two rings are held together by four μ^2-P bridges (shown in pale gray in Figure 2) between neighboring top and bottom Cu atoms. The Cu–μ^2-P–Cu angles within the eight-membered ring are larger (Cu1–P3–Cu4A 114.89(14) °) than those between the rings (Cu1–P1–Cu2 81.00(10), Cu3–P2–Cu4 103.00(12) °), also in the case of the minor components of the disordered atoms Cu4–b and Cu4A–b (Cu1–P3–Cu4A_b 88.65(13) vs Cu3–P2–Cu4_b 77.46(12) °). The distances of the major components of the disordered Cu4 and Cu4A to Cl4 (Cl4–Cu4 3.561 Å) are longer, those of the lesser occupied positions Cu4_b and Cu4A_b shorter (2.551(3) Å). The distances of Cu4_b to P2 and Cu3 are also short (2.208(2), 2.776(4) Å) while the bond Cu4_b–Cl3 is longer than Cu4_a–Cl3 (2.349(4) vs. 2.241(3) Å). Including the contacts to Cl4, all Cu atoms are 4-fold coordinated, Cu1, Cu1A, Cu4 and Cu4A by two P and two Cl, the other by one P and 3 Cl atoms. In addition, there are short Cu···Cu distances between μ^2-P bridged copper atoms of the upper and lower ring (Cu1···Cu2 2.909(2), Cu3–Cu4_a 2.776 Å), which might be an indication of weak cuprophilic interactions between the rings, whereas the distances of the μ^2-P bridged copper atoms within the rings are longer (Cu1···Cu4A 3.785 Å). The Cu–Cl bond lengths in the linear anion (2.095(4) Å) correspond to average values of the dichlorocuprate(I) anion [14] and are shorter than in $CuCl_2 \cdot 2\,H_2O$ (2.290(4) Å).[15] The presence of $[Cu^{I}Cl_2]^-$ is compatible with the demands of charge compensation. Furthermore, $Cu^{II}Cl_2$, with its paramagnetic d^9-electron configuration, can be excluded by the appearance of the ^{31}P signal in the NMR spectrum. The THF molecules are disordered and display no strong interactions with the metal. The only short Cu–O distance is 2.337(1) Å (Cu4_a O2). This is in accordance with the facile loss of THF from **2a,b**·4THF under vacuum or during prolonged storage without mother liquor.

The THF-soluble dimeric bis(benzazaphosphole)CuX complexes have simpler structures. Complex **3b** (Figure 3),

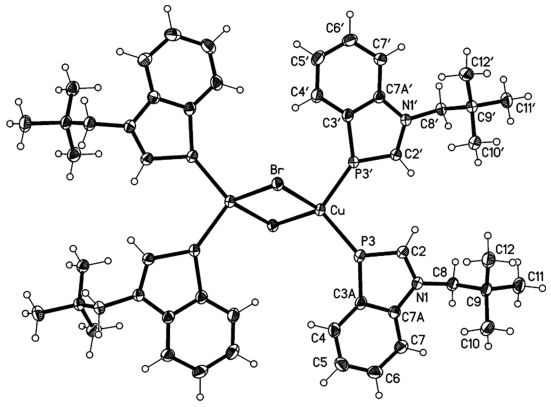

Figure 3. Structure of **3b** in the crystal (ellipsoids with 50% probability). Selected bond lengths (Å) and angles (°): Cu–Br 2.5372(4), Cu–Br# 2.4817(4); Cu#–Br–Cu 83.748(13), Br#–Cu–Br 96.252(12), P(3)–Cu–Br 121.57(2), P(3′)–Cu–Br 102.465(18), P(3)–Cu–Br# 113.586(19), P(3′)–Cu–Br# 117.107(19); for further data see Table 1.

crystallized by slow concentration of the dcm solution of the soluble products of the reaction of **1** and CuBr (reactant ratio 1:1), is a μ^2-Br bridged dimer with two η^1-P coordinated ligands at each Cu atom, and it is isotypic with the recently reported silver chloride complex of **1**.[10a] The triclinic unit cell, space group $P\bar{1}$, accommodates one molecule, which thus possesses crystallographic inversion symmetry. The benzazaphosphole ligands in **3b** are coordinated in a tilted mode. The two ligands display bend angles of 29.3 and 8.1°, respectively, between the Cu–P vector and the ring planes. This corresponds to deviations of 1.11 and 0.30 Å of Cu from this plane. Crystals of the analogously prepared CuCl complex displayed weak and diffuse X-ray diffraction patterns that did not allow meaningful refinement, but since the NMR spectra of the products are very similar, an analogous structure can be anticipated. It is noteworthy that this structure is based on the known gas phase dimeric structure of CuX.[16] An alternative dimeric structure with the same benzazaphosphole/CuBr ratio of 2:1 is represented by complex **4b** (Figure 4). Its crystals were grown by

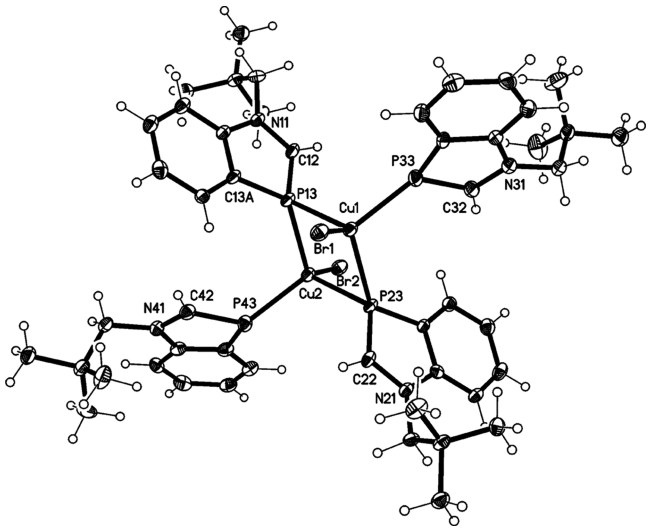

Figure 4. Structure of **4b** in the crystal (ellipsoids with 50% probability). Selected bond lengths (Å) and angles (°): Cu1–Br1 2.4038(6), Cu2–Br2 2.4000(6); P33–Cu1–Br1 109.36(3), P23–Cu1–Br1 110.20(3), P13–Cu1–Br1 107.63(3), P43–Cu2–P13 111.50(4); for further data see Table 1.

diffusion of hexane into a concentrated solution of the soluble products obtained from **1** and excess CuBr (reactant ratio 1:3) in THF. The crystal structure analysis shows the monoclinic space group $P2_1/n$ with four dimers in the unit cell (and no imposed crystallographic symmetry). The two copper atoms of **4b** each coordinate two benzazaphosphole ligands, the ligands L1 and L2 in a μ^2-P, the ligands L3 and L4 in a bent η^1-P mode, and the bromides in terminal positions. The bend angles of L3 and L4 amount to 27.6 and 32.7°, corresponding to deviations of 1.04 and 1.24 Å of the Cu atoms from the ring planes. The μ^2-P ligands necessarily coordinate the two Cu(I) atoms outside the ligand ring plane, but not symmetrically. The smaller deviations (1.12 and 1.16 Å for L1/Cu2 and L2/Cu1 respectively) correspond to bend angles of 29.3 and 30.6 °, similar to those of the two η^1-P ligands, while the others (1.55 and 1.58 Å for L2/Cu2 and L1/Cu1, respectively) correspond to bend angles of 41.3 and 40.0°. Finally, it should be mentioned that the μ^2-P coordination mode leads to a much shorter intra-annular Cu···Cu distance in **4b** than the μ^2-Br coordination in **3b** (see Table 1), indicating that cuprophilic interactions might be operative in the system – see below.

The same compound, but with slight structural changes (**4b**′, Figure S9), was obtained from the oversaturated CD_3OD

DOI: 10.1021/ic502367d
Inorg. Chem. 2015, 54, 2117–2127

Table 1. Comparison of Characteristic Bond Lengths (Å) and Angles (°)[a]

	2a·4THF	3b	4b	4b′	5a·2MeOH	5b·2MeOH
η^1-P−Cu	-	2.2531(6), 2.2649(6)	2.2809(12), 2.2917(12)	2.2886(15)	2.2470(4)	2.2436(4)
μ^2-P−Cu	2.229(4)[b]− 2.345(4)	-	2.3117(10)− 2.3793(10)	2.3145(12)− 2.3975(11)	2.3226(4)− 2.3360(4)	2.3266(4), 2.3306(4)
P−Cu−P′	117.47(13)− 124.19(11)	105.92(2)	108.89(4)− 112.12(4)	108.12(3)− 111.61(4)	107.656(17)− 110.384(13)	108.193(16)− 111.054(12)
Cu−μ2-P−Cu	see text	-	71.04(3)	71.88(3)	69.616(13)	68.946(12)
Cu···Cu#	2.909−3.785[c] 3.215−3.651[d]	3.3504(6)[d]	2.7259(7)[c]	2.7665(10)[c]	2.6593(4)[c]	2.6361(3)[c]
P−C2	1.721(11)	1.714(2)	1.716(4)	1.691(5)	1.7161(15)	1.7125(15)
P−C3a	1.783(9)	1.775(2)	1.773(4)	1.772(4)	1.7656(15)	1.7631(14)
N−C2	1.326(12)	1.360(3)	1.351(5)	1.355(5)	1.3500(19)	1.3528(18)
N−C7a	1.404(11)	1.385(3)	1.396(5)	1.389(5)	1.3936(19)	1.3957(18)
C3a−C7a	1.399(12)	1.417(3)	1.412(5)	1.403(5)	1.411(2)	1.4131(19)
C2−P−C3a	89.7(5)	89.12(10)	89.71(17)	89.5(2)	90.30(7)	90.44(7)
P−C2−N	114.5(7)	115.19(15)	114.7(3)	115.5(3)	113.69(11)	113.85(11)

[a]The bond lengths and angles of the benzazaphosphole rings refer to the ligands L1 (those with P1 (**2a**·4THF) or P3 or P13). Average deviation of the benzazaphosphole ring atoms from ring plane (Å): for **3b** 0.009 (L1), 0.023 (L2), **4b** 0.012 (L3, L4) to 0.014 (L2), **5a** 0.012 (L1), 0.027 (L2) and **5b** 0.011 (L1), 0.028 (L2). The values for the μ^2-P bound ligands are similar. [b]The distance from the weakly occupied Cu4_b to P2 is 2.208(2) Å. [c]Refers to the μ^2-P bridging Cu···Cu distance (range) (Å). [d]Refers to the μ^2-X bridging (X = Cl, Br) Cu···Cu distance (range) (Å).

solution of the soluble products, formed from equimolar amounts of **1** and CuBr in THF and subjected to X-ray structure analysis at room temperature. It crystallized in the primitive monoclinic lattice *P*21/*c* with two inversion-symmetric molecules in the unit cell, which corresponds to the halved subcell of the low-temperature determination **4b**. There is no sign of disorder in **4b′**. On cooling, therefore, the molecular inversion symmetry is lost and the ring substituents display slightly different orientations. The structure **4b′** is also distinguished by its increased Cu···Cu distance (by 0.0406(10) Å), a lengthening of the longer Cu−μ^2-P bridging bond (by 0.0182 and 0.0203(10) Å) and a shortening of the Cu−Br bonds (to 2.3861 (8) Å). The differences emphasize the unsymmetric Cu−μ^2-P bridging bond and may be attributed to measuring at different temperatures. Other differences are marginal (Table 1).

Similar μ^2-P bridging structures were found for crystals of the bis(benzazaphosphole) copper(I) halides **5a**·2MeOH (Figure 5) and 5**b**·2MeOH (Figure 6), obtained from the soluble products

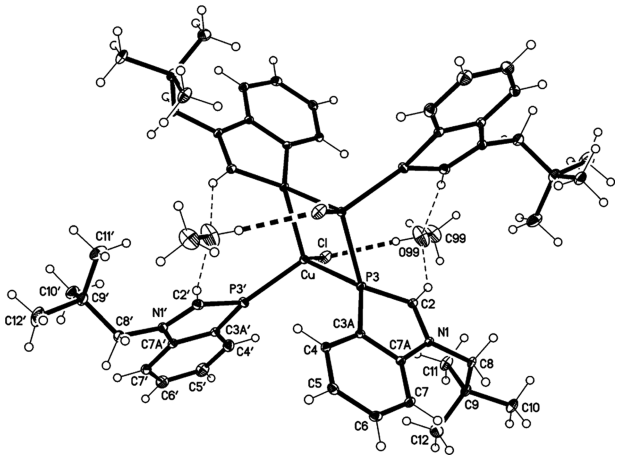

Figure 5. Structure of **5a**·2MeOH in the crystal (ellipsoids with 30% probability). Selected bond lengths (Å) and angles (°): Cu−Cl 2.2597(4); P3′−Cu−Cl 110.703(18), Cl−Cu−P3 111.660(16), Cl−Cu−P(3)#1 107.103(16); O99−H99 0.82(3), H99···Cl 2.32(3), O99···Cl 3.1281(18), O99−H99−Cl 172(3); for further data see Table 1.

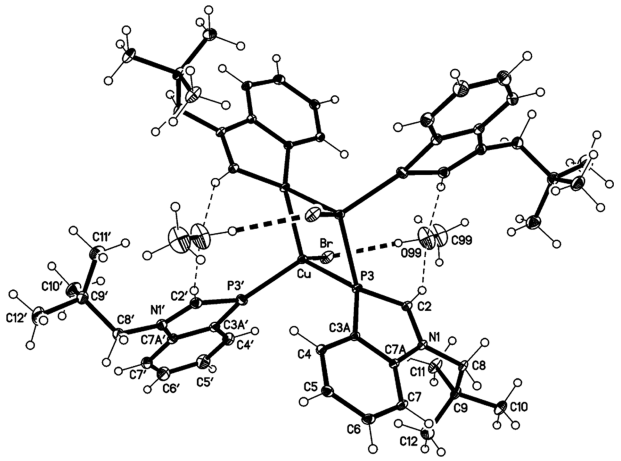

Figure 6. Structure of **5b**·2MeOH in the crystal (ellipsoids with 50% probability). Selected bond lengths (Å) and angles (°): Cu−Br 2.3889(2); P3′−Cu−Br 110.381(14), Br−Cu−P3 110.187(12), Br−Cu−P(3)#1 107.083(12); O99−H99 0.92(3), H99···Br 2.36(3), O99···Br 3.2786(19), O99−H99−Br 173(3); for further data see Table 1.

of incomplete reactions of **1** with excess CuX, reactant ratio 1:3. In these two isotypic compounds (monoclinic, space group $P2_1/c$, two dimers per cell, imposed inversion symmetry), methanol is bound via hydrogen bonds to the terminally coordinated halides. The Cu···Cu distance is significantly shorter than in **4b** and **4b′**, and the η^1-P−Cu bonds are also shorter. The μ^2-P bridging bond is symmetric with equal deviations of the Cu atoms from the ring planes, 1.22 and 1.25 Å for **5a**·2MeOH and **5b**·2MeOH, corresponding to bend angles of 31.9 and 32.6 °. The bend angles of the η^1-P bound ligands (11.3, 10.0 °, Cu deviations 0.40 and 0.35 Å) are smaller than in **4b**. The bond lengths and angles of the ligand in **5a**·2MeOH and **5b**·2MeOH are similar to those in **2a**, **3b**, and **4b**, and they are only slightly altered compared to the values in free **1**.[11]

The obvious avoidance of η^1-P coordination of Cu(I) within the ring plane of the benzazaphosphole ligands and the exclusive coordination in μ^2-P and/or bent η^1-P modes distinguishes the benzazaphosphole CuX complexes markedly

DOI: 10.1021/ic502367d
Inorg. Chem. 2015, 54, 2117−2127

from phosphinine CuX complexes, which prefer coordination of copper within the ring plane.[3,17] The only exceptions so far are a sterically distorted bis(pyridyl)phosphinine CuBr pincer complex[18] and, here more relevant, a bis(2-hydroxyphosphinine)CuCl dimer with μ^2-P and slightly bent η^1-P coordination,[19] structurally similar to **3b**. Possibly this is associated with the +M-effect of the *o*-OH group and an increased π-density at the low-coordinated phosphorus. μ^2-P in combination with μ^2-Br coordination was also found in a [bis(phosphonio)-isophosphindolide]$^+$ $[Cu_2Br_3]^-$ complex.[20] The 10π-aromatic ligand in this compound contains a formally positively charged σ^2-P, however with high π-density, provided by the two ylidic carbon atoms in α-position. This results in a comparable electronic environment to that in the benzazaphosphole ligands and in similar coordination properties. The P−Cu bond lengths in the isophosphindolide Cu_2Br_3 complex are similar to those in **4b** and **4b′**; that is, the μ^2-P bridge to the Cu_2 pair is asymmetric, the Cu···Cu distance is short, and the bond lengths and angles of the ligand are not significantly changed by the coordination. The asymmetric bridge was explained similarly to the 3-center-2-electron bonds of copper aryls[21] by stronger L(σ)−M than L(π)−M interactions. A 4-electron donor role of the benzazaphosphole ligands, with two 2-center-2-electron bonds to Cu(I), corresponding to sp^3-hybridization at phosphorus, can be excluded, as this, in contrast to the experimental findings, is likely to result in loss of aromaticity of the ligand and substantial changes of the bond lengths within the five-membered ring. An example of this coordination type is a structurally characterized dimeric cyclopentadienylnickel benzazaphospholide complex.[22]

DFT Studies of the P−Cu Bonds in 4b. To investigate the coordination modes of the ligand to CuBr, we first considered a 1:1 complex. Geometry optimization at the ωB97xD/cc-PVDZ level resulted in two different structures **I** and **II** (Figure S10 of the Supporting Information), with nearly identical energies. Whereas in **I**, the ligand is bound nearly in plane with the copper atom of CuBr, the CuBr unit in **II**, which is more stable than **I** by 0.9 kcal/mol, is bound in an η^2 fashion to the π-system. The binding energy of **I** is 39.0 kcal/mol. It is noteworthy that the NICS(0) value[23] of −11.5 ppm, calculated for **1** at the b3lyp/cc-pvdz//ωB97xD/cc-PVDZ level, is only slightly influenced upon complexation (−12.2 and −9.7 ppm for **I** and **II**, respectively), indicating that the interaction with copper has only a minor effect on the electronic structure of the ligand—quite surprisingly even in the case of **II**. **I** can then be complexed again in an η^2 manner by a second CuBr unit, resulting in a 1: 2 complex **III** (See Figure S11 in the Supporting Information) with one in plane and one out of plane CuBr. The binding energy of the second (out of plane) CuBr unit to **I** is 36.5 kcal/mol. The similar values for the first and the second complexation indicates that the two processes are nearly independent of each other. This observation is in further agreement with the small variation of the NICS values as discussed above. On the other hand, complexation of **I** by a second ligand (**1**) results in a structure (**IV** − see Figure S12 in the Supporting Information), with one in-plane and one out-of-plane ligand, and an overall stabilization (with respect to two ligands and one CuBr unit) of 58.7 kcal/mol only. Clearly, the binding energy of the second ligand is reduced here with respect to that of the first one. It should be mentioned that a further L_2CuBr structure, with both ligands in an in-plane position, could also be optimized, but this structure is less stable than **IV** by 5.3 kcal/mol.

For a more detailed picture of the formation of dimers, quantum chemical calculations on **3b** and **4b** were performed. It should be noted that optimization of the molecules **3b** and **4b** at the ωB97xD/6−31G* and also at the ωB97xD/cc-PVDZ levels resulted in somewhat modified structures (the ωB97xD/cc-PVDZ optimized molecular structures $\mathbf{3b_{OM}}$ and $\mathbf{4b_{OM}}$ are shown as Figure S13 of the Supporting Information). An important feature of these structures is the close contact between the aromatic rings, presumably experiencing intramolecular π-stacking, which is more effective in the absence of intermolecular forces acting in the crystal, although weak π-interactions are suggested also in **4b** by an intermolecular contact of 3.70 Å between the centers of the aromatic rings (C14−17, C14a, C17a) and (C24−C27, C24a, C27a), operator *b* translation, interplanar angle 1 degree, offset ca. 1.3 Å. The optimized structure of $\mathbf{4b_{OM}}$ turned out to be more stable than $\mathbf{3b_{OM}}$ by 8.4 kcal/mol. The overall stabilization in $\mathbf{4b_{OM}}$ with respect to four ligands and two CuBr units is 150.9 kcal/mol. The stabilization in $\mathbf{4b_{OM}}$ with respect to the L_2CuBr system (two molecules of **IV**) is 33.5 kcal/mol. Therefore, although the entropy factor reduces the relative stability of $\mathbf{3b_{OM}}$ and $\mathbf{4b_{OM}}$ with respect to two monomers **IV** by about 10 kcal/mol at room temperature in terms of Gibbs free energy, the tetracoordination of Cu(I) is clearly preferred. In THF solution, the tetracoordination can also be achieved by the involvement of solvent molecules. The ωB97xD/cc-PVDZ complexation energy between **IV** and one THF amounts to 15.8 kcal/mol (for the optimized complex, see Figure S14 of the Supporting Information). The weak interactions with THF and the much lower bonding energy of a second compared to the first ligand in **IV** suggests that this stabilization is not too strong. It might be sufficient, however, to compete with the dimerization to $\mathbf{3b_{OM}}$ and $\mathbf{4b_{OM}}$ and to cause the kinetic lability, rapid ligand exchange reactions, and the solubility in THF. The formation of the crystalline dimers **4b** (and **3b**) can then be attributed to decreasing activity of coordinating solvent and additional stabilization of the dimers by the interactions in the crystal. A further important result comes from the b3lyp/cc-pvdz NICS calculation on $\mathbf{4b_{OM}}$, resulting in −11.2 ppm for the bridging and −12.8 ppm for the tilted terminal ligand. These results show that, as in the case of the 1:1 complexes **I** and **II**, the aromaticity of the ligand is only slightly altered in any of the two different coordination modes.

Further calculations on **4b**, using the geometry observed in the crystal, targeted insight into the P−Cu bonding contributions, particularly in the PCu_2 cores. The short Cu···Cu distance in **4b** suggests Cu···Cu interactions within the molecule. The AIM analysis,[24] carried out for the ωB97xD/6−31G* electron density of **4b** at the crystal structure geometry, showed however no bond critical points between the two copper atoms. Because it has been shown[25] recently that the existence of the bond critical point and the electron density value strongly depends on the theoretical level used, we have carried out the calculations with different basis sets, with and without diffuse functions including the 6−31G*, 6−311+G**, and cc-PVDZ basis sets, but in no case were bond critical points obtained. This contrasts with the detection of Cu···Cu interactions by bond critical points in the μ^2-P coordinated $L_2(CuOac)_4$ complex of the same ligand.[10b] A possible explanation is that the two phosphorus atoms in the four-membered ring repel each other strongly because of the interaction between their in-plane lone pairs, increasing the P···P and necessarily decreasing the Cu···Cu distance. Despite the decreased distance, however,

DOI: 10.1021/ic502367d
Inorg. Chem. 2015, 54, 2117−2127

no significant electron density can develop at the center of the four-membered ring as a consequence of the electron density from the phosphorus lone pairs, which is the reason for the repulsive P···P interaction.

The most important information for the molecular structure came from the inspection of the molecular orbitals. The HOMO is composed of Cu d orbitals and the π-type HOMO of the bridging ligand (Figure 7), showing the involvement of

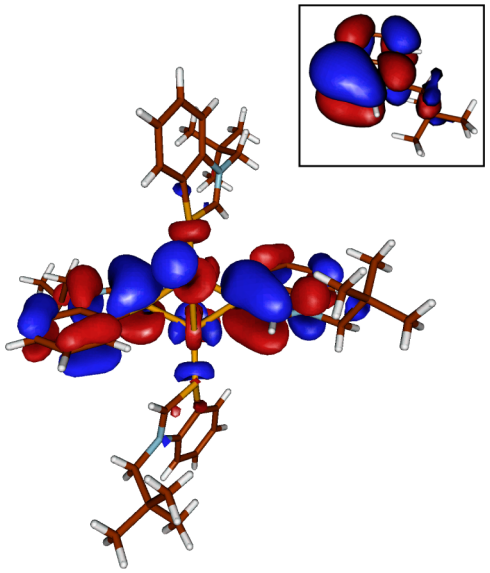

Figure 7. ωB97xD/cc-PVDZ Kohn−Sham HOMO of **4b**, composed from the π-HOMO of the ligand, having a significant contribution at phosphorus as shown in the insert, and the Cu orbitals.

the ligand π-systems in the complex formation. It is particularly noteworthy that the π-type HOMO of the ligand remains nearly unchanged upon complexation. This is in agreement with the small changes in the NICS values. Lacking direct Cu···Cu interactions, it seems apparent that the structure is held together by the bridging ligands. In order to study this bonding situation further we carried out a Natural Resonance Theory analysis on the basis of the Natural MOs. Although we explicitly searched for 3c interactions, no such interaction was found. Clearly the delocalized π-system, which acts as donor orbital, differs significantly from the lone pair as donor in 3c−2e bonding.

CONCLUSIONS

N-Substituted *1H*-1,3-benzazaphospholes, represented by **1**, react in THF at room temperature with copper(I) halides to form kinetically labile complexes. The initially formed products are soluble, undergo rapid ligand exchange reactions and convert slowly to more stable insoluble products that precipitate from the equilibrium mixture. In the case of **1** and THF as solvent these are **2a**·4THF and **2b**·4THF. Suitably timed separation of the transiently formed soluble products from unconverted CuX and insoluble **2a,b**·4THF allows crystallization of $[(L_2CuX)_2]$ species from concentrated solutions and identification of the complex types **3**−**5**. The growth of single crystals, even of the insoluble complexes **2a,b**·4THF, from a suitable filtrate gives evidence that the formation of these compounds does not require the presence of CuX and can be attributed to slow solubility-driven formation from dissolved labile complexes. The final conversion of temporarily formed labile complexes in solution to **2a,b**·4THF is proved by the general high yield of these complexes (with respect to the yield-limiting reactant) after sufficient reaction time, even for the 2:1 reactant ratio of **1** and CuX, which otherwise should favor the $[(L_2CuX)_2]$ complexes. The observation of only μ^2-P and/or bent η^1-P coordinated benzazaphosphole ligands in the Cu(I) complexes, contrasting with the preferred η^1-P coordination of phosphinine CuX complexes with Cu within the ring plane, gives evidence that the π-excess nature and the different electronic structure of the benzazaphospholes have a strong impact on the nature of the bond between the low-coordinated phosphorus and the transition metal. A closer insight into the reasons for the lability and the peculiar bonding situation of these complexes is achieved by DFT calculations. These show also two types of monomeric LCuBr complexes, one with the usual η^1-L and a slightly more stable one with η^2-L coordination. Both are able to coordinate a second CuBr with a similar gain of energy as for the first CuBr, whereas the interaction energy of LCuBr with a second ligand is lower. This hints toward the higher stability of the copper-rich complexes **2a,b** and their final preference. Because dimerization of L_2CuBr, resulting in the favorable tetracoordinated Cu(I) complexes, and stabilizing effects by crystal forces are also energetically beneficial, such complexes are formed under kinetically controlled conditions. Competing interactions of L_2CuBr with the THF solvent and the entropy factor of the dimerization result in lability and a delicate balance between the different complexes. The particular bonding situation in **4b** arises by conservation of the delocalized π-system and involvement of the π-type HOMO of the ligand in the bonding, and differs significantly from classic lone-pair-based 3c−2e interactions. This is in accordance with the minor changes of the ligand bond lengths and NICS values upon coordination. A noteworthy feature is that, despite the rather short Cu···Cu distance in **4b**, no bond critical point could be located between the metal atoms. This means that the short Cu···Cu contacts are not necessarily attributable to weak bonding interactions between the copper atoms, as detected for the $L_2(CuOAc)_4$ cluster[10b] with the same ligand and similar Cu···Cu distances. A plausible explanation is the repulsion of the in-plane P electron lone pairs of the two μ^2-P bridging ligands in the small four-membered ring of **4b**. This increases the P···P distance, resulting in a shortened Cu···Cu distance, and also may cause the unsymmetric bridging and contribute to destabilization of the dimers compared to the $[L_6Cu_8X_7][CuX_2]$ cluster complexes with larger rings and smaller L:CuX ratio.

The above results show that π-electron rich σ^2-P ligands exhibit distinct coordination properties compared to σ^2-P phosphinine or σ^3-P phosphane ligands and offer access to novel types of P-coordinated transition metal complexes.

EXPERIMENTAL SECTION

General Remarks. All synthetic procedures and NMR measurements were carried out under dry argon in carefully dried, freshly distilled solvents using standard Schlenk techniques and glassware heat-dried in vacuum. 1-Neopentyl-1,3-benzazaphosphole (**1**) was synthesized by a modification of a known procedure,[11] using Me_3SiCl (ca. 1 equiv) to accelerate the final cyclocondensation of *o*-phosphanyl-*N*-neopentylaniline with dimethylformamide dimethylacetal. This shortens the reaction time at 50 °C from 7 days to 1 day, yield 76%. Crystalline, almost colorless CuCl and CuBr (crystal size mainly 0.01 to 0.5 mm) were prepared by known methods.[26] $Cu(SMe_2)Br$ was used as purchased (AlfaAesar, 97%). Elemental analyses of solid products were determined with a Vario Micro Cube CHN analyzer

DOI: 10.1021/ic502367d
Inorg. Chem. 2015, 54, 2117−2127

from Elementar under standard conditions. NMR spectra were measured on a multinuclear FT-NMR spectrometer ARX300 (Bruker) at 300.1 (^{1}H), 75.5 (^{13}C), and 121.5 (^{31}P) MHz. Chemical shifts δ are given in ppm. Shift references are tetramethylsilane for ^{1}H and ^{13}C and H_3PO_4 (85%) for ^{31}P or solvents calibrated to these standards. Coupling constants refer to J_{HH} in the proton and to J_{PC} in the ^{13}C NMR spectra unless indicated otherwise. HRMS spectra were measured on a 7T Fourier transform ion cyclotron resonance mass spectrometer APEX IV (Bruker Daltonics) (ESI in MeOH or MeOH/formic acid).

Reaction of 1 with CuCl (Reactant Ratio 2:1). Filtration of the suspension formed from **1** (416 mg, 2.02 mmol) and CuCl (100 mg, 1.01 mmol) in THF after 4 days, washing with THF and evaporation of the solvent under vacuum (ca. 15 min, 1 Torr) gave **2a**·2.8 THF (0.46 THF/ligand) as a yellow powder, yield 225 mg (94% rel. to CuCl). This is insoluble or sparsely soluble in common organic solvents such as diethyl ether, dichloromethane, $CHCl_3$, benzene, methanol, or acetone and in water, but soluble in DMSO. Removal of the solvent from the filtrate provided a pale yellow viscous substance (297 mg), δ^{31}P($CDCl_3$) = 65.4, which from a small amount of MeOH gave crystals of excess **1** (210 mg, 51%), identified by the known unit cell parameters.[11] **2a**·2.8 THF – ^{1}H NMR (D_6-DMSO): δ = 0.90 (s, 9 H, CMe_3), 4.26 (br s, 2 H, NCH_2), 7.22 (br td, ^3J = 7.6, $^4J_{PH}$ = 2.6 Hz, 1 H, H-5), 7.43 (t, ^3J = 8.3, 7.2 Hz, unresolved fine splitting $^4J \approx {}^5J_{PH} \approx$ 1 Hz, 1 H, H-6), 7.96 (superimposed d, ^3J = 8.7 Hz, 1 H, H-7), 7.96 (superimposed t, ^3J = 7.6, $^3J_{PH}$ = 6.8 Hz, 1 H, H-4), 8.68 (d, $^2J_{PH}$ = 36.3 Hz, 1 H, H-2); 1.74 (m, CH_2, 0.46 THF), 3.59 (m, OCH_2, 0.46 THF). ^{13}C{^{1}H} NMR (D_6-DMSO): δ = 27.67 (s, CH_3), 34.05 (s, CMe_3), 59.93 (s, NCH_2), 115.12 (s, C-7), 121.17 (d, ^3J = 13.3 Hz, C-5), 125.26 (d, ^2J = 2.7 Hz, C-6), 127.97 (d, ^2J = 15.9 Hz, C-4), 134.91 (d, ^1J = 4.0 Hz, C_q-3a), 142.90 (s, C_q-7a), 157.98 (d, ^1J = 10.6 Hz, C_q-2); 25.10 (s, CH_2, THF), 67.00 (s, OCH_2, THF). ^{31}P NMR (D_6-DMSO): δ = 35.9 (s). The CHN analysis displayed loss of THF during storage. Anal. Calcd for **2a**, $C_{72}H_{96}Cl_9Cu_9N_6P_6$ (2122.41): C, 40.74; H, 4.56; N, 3.96. Found: C, 40.40; H, 4.61; N, 3.94.

Reaction of 1 with CuBr (Reactant Ratio 2:1). Filtration of the suspension formed from **1** (368 mg, 1.80 mmol) and CuBr (129 mg, 0.90 mmol) in THF after 4 days and evaporation of the solvent under vacuum gave 250 mg of **2b**·0.9 THF (yield 97% rel. to CuBr) as a yellow powder with the same solubility properties as described for **2a**. Removal of the solvent from the filtrate furnished a viscous residue (264 mg), δ^{31}P = 68.6, from which unconverted **1** was recovered by crystallization from methanol (ca. 240 mg, 65%). **2b**·0.9 THF is sparsely soluble in CD_3OD and led to extraction and strong signals of THF while only a trace of **2b** was indicated. The THF-free residue was then dissolved and measured in D_6-DMSO. ^{1}H NMR: δ = 0.91 (s, 9 H, CMe_3), 4.26 (br s, 2 H, NCH_2), 7.22 (br td, ^3J = 7.2, $^4J_{PH}$ = 2.6 Hz, 1 H, H-5), 7.43 (t, ^3J = 8.4, 6.8 Hz, unresolved fine splitting $^4J \approx {}^5J_{PH} \approx$ 1 Hz, 1 H, H-6), 7.94 (d, ^3J = 8.7 Hz, 1 H, H-7), 8.34 (br t, ^3J = 7.8, $^3J_{PH}$ = 6.8 Hz, 1 H, H-4), 8.67 (d, $^2J_{PH}$ = 35.9 Hz, 1 H, H-2). ^{13}C{^{1}H} NMR: δ = 27.71 (s, CH_3), 34.11 (s, CMe_3), 60.03 (s, NCH_2), 115.11 (s, C-7), 121.18 (d, ^3J = 11.9 Hz, C-5), 125.34 (d, ^2J = 2.7 Hz, C-6), 128.30 (d, ^2J = 15.9 Hz, C-4), 134.91 (br s, C_q-3a), 143.05 (s, C_q-7a), 158.02 (d, ^1J = 11.9 Hz, C_q-2). ^{31}P NMR: δ = 32.9 (s). Anal. Calcd for **2b**·0.9 THF, $C_{75.6}H_{103.2}Br_9Cu_9N_6O_{0.9}P_6$ (2565.73): C, 35.09; H, 4.02; N, 3.25. Found: C, 34.91; H, 4.11; N, 3.31.

Preparation of Crystals of 2a·4THF. Filtration of the suspension formed from **1** (92 mg, 0.45 mmol) and CuCl (89 mg, 0.90 mmol) in THF after 20 h and removal of the solvent from the filtrate gave 97 mg of a yellow viscous residue. ^{1}H NMR (CD_3OD): δ = 0.92 (s, 9 H, CMe_3), 4.13 (s, 2 H, NCH_2), 7.12 (br td, ^3J = 8, 7, $^4J_{PH}$ = 1.8 Hz, 1 H, H-5), 7.38 (br dd, ^3J = 8.7, 7, 1 H, H-6), 7.75 (d, ^3J = 8.7 Hz, 1 H, H-7), 7.88 (br t, ^3J = 8, $^3J_{PH}$ = 5 Hz, 1 H, H-4), 8.47 (d, $^2J_{PH}$ = 36.6 Hz, 1 H, H-2). ^{13}C{^{1}H} NMR (CD_3OD): δ = 28.70 (s, CH_3), 35.51 (s, CMe_3), 61.86 (s, NCH_2), 115.77 (s, C-7), 121.99 (d, ^3J = 13.3 Hz, C-5), 126.11 (DEPT d, ^4J = 2.2 Hz, C-6), 129.90 (d, ^2J = 18.6 Hz, C-4), 145.05 (d, ^2J = 4.0 Hz, C_q-7a), 163.35 (d, ^1J = 30 Hz, C-2); C_q-3a signal at noise level. ^{31}P{^{1}H} NMR (CD_3OD): δ = 51.4 (vbr). HRMS (ESI in MeOH): calcd for L_2Cu^+ $[C_{24}H_{32}Cu_1N_2P_2]^+$, 473.1332; found, 473.1331 and correct isotopic pattern. Overlayering of a concentrated solution in THF with *n*-hexane provided yellow crystals of **2a**·4THF. A suitable crystal was measured by XRD. Selected bond lengths and angles are compiled in Table 1, crystal data in Table 2. Separation of residual crystals by filtration and prolonged drying under vacuum furnished **2a**. Anal. Calcd for $C_{72}H_{96}Cl_9Cu_9N_6P_6$ (2122.41): C, 40.74; H, 4.56; N, 3.96. Found: C, 41.34; H, 4.43; N, 3.97.

Preparation of Crystals of 3b. Tetrahydrofuran (5 mL) was added to a mixture of **1** (143 mg, 0.70 mmol) and CuBr·SMe_2 (143 mg, 0.70 mmol). The solid starting materials dissolved initially to give a yellow solution. Beginning after about 2 min, a yellow suspension was formed. This was filtered after 14 h at 22 °C, and the precipitate was washed with THF (5 mL). Removal of solvent under vacuum (ca. 1 Torr, 20 min) gave 193 mg of yellow powder **2b#** (93% rel. to CuBr) and 73 mg of pale yellow viscous residue. Slow evaporation of the solvent from a solution of the latter in CD_2Cl_2 provided crystals of **3b**. Selected bond lengths and angles are compiled in Table 1, crystal data in Table 2. ^{1}H NMR (CD_2Cl_2): δ = 0.99 (s, 9 H, CMe_3), 4.10 (br s, 2 H, NCH_2), 7.16 (tdd, ^3J = 7.9, 7.2, $^4J_{PH}$ = 2.3, ^4J = 1.1 Hz, 1 H, H-5), 7.38 (tt, ^3J = 8.3, 7.2, $J+J'$ = 2.7 Hz, 1 H, H-6), 7.63 (dq(unres.), ^3J = 8.3 Hz, 1 H, H-7), 8.07 (dddd, ^3J = 7.2, $^3J_{PH}$ = 6.8, ^4J = 1.5, ^5J = 0.8 Hz, 1 H, H-4), 8.47 (d, $^2J_{PH}$ = 37.0 Hz, 1 H, H-2). ^{13}C{^{1}H} NMR (CD_2Cl_2): δ = 28.40 (s, CH_3), 34.77 (s, CMe_3), 61.28 (s, NCH_2), 114.11 (s, C-7), 120.39 (d, ^3J = 13.3 Hz, C-5), 124.87 (d, ^4J = 2.7 Hz, C-6), 129.42 (d, ^2J = 19.9 Hz, C-4), 140.56 (d, ^1J = 29.2 Hz, C_q-3a), 143.78 (d, ^2J = 4.0 Hz, C_q-7a), 162.52 (d, ^1J = 39.8 Hz, CH-2). ^{31}P NMR (CD_2Cl_2): δ = 61.2. (For preparation of crystals of **3b** by 1:1 reaction of **1** and CuBr see Supporting Information, Tables S1 and S2.)

2b#: The ^{1}H and ^{13}C NMR data are in good agreement with the data given above for **2b**·0.9 THF. ^{31}P NMR (D_6-DMSO): δ = 43.2 (br s). Anal. Calcd. for $C_{72}H_{96}Br_8Cu_8N_6P_6$ (2379.02): C, 36.35; H, 4.07; N, 3.53. Found: C, 36.08; H, 4.33; N, 3.75.

Preparation of Crystals of 4b. Filtration of the suspension formed from **1** (97 mg, 0.47 mmol) and CuBr (202 mg, 1.41 mmol) in THF after ca. 1 day and removal of the solvent from the filtrate under vacuum gave a yellow viscous residue (ca. 270 mg). The ^{1}H and ^{13}C NMR data in CD_3OD (see Table S2) are similar to those of the above precursor of **3b**; ^{31}P NMR (CD_3OD): δ = 63.7 (vbr). Slow diffusion of overlayered hexane into a concentrated solution of this residue provided very small and thin crystals. A suitable crystal allowed crystal structure analysis. Selected bond lengths and angles are compiled in Table 1, crystal data in Table 2.

Preparation of Crystals of 4b′. The suspension formed from **1** (311 mg, 1.51 mmol) and CuBr (217 mg, 1.51 mmol) in THF after 4 days was filtered and washed with THF to give 317 mg **2a**·3.1 THF, see Table S1, NMR data Table S2). The solvent of the filtrate (183 mg viscous residue) was replaced by CD_3OD. Storage of the NMR sample, ^{31}P NMR (CD_3OD): δ = 67.4, for ca. 4 weeks led to formation of colorless crystals of **4b′**. Selected bond lengths and angles are compiled in Table 1, crystal data in Table 2. NMR data of separated crystals -^{1}H NMR ($CDCl_3$): δ = 0.94 (s, 9 H, CMe_3), 4.11 (br s, 2 H, NCH_2), 7.16 (tdd, ^3J = 8, 7.2, $^4J_{PH}$ = 2.3, ^4J = 1 Hz, 1 H, H-5), 7.37 (tt, ^3J = 8.3, 7.2, $J+J'$ = 2.2 Hz, 1 H, H-6), 7.63 (br d, ^3J = 8.3 Hz, 1 H, H-7), 8.07 (br dd, ^3J = 7.9, $^3J_{PH}$ = 4.9 Hz, 1 H, H-4), 8.47 (d, $^2J_{PH}$ = 36.6 Hz, 1 H, H-2). ^{13}C{^{1}H} NMR ($CDCl_3$): δ = 28.15 (s, CH_3), 34.39 (s, CMe_3), 60.94 (s, NCH_2), 113.53 (s, C-7), 120.06 (d, ^3J = 11.9 Hz, C-5), 124.51 (s, C-6), 129.08 (d, ^2J = 19.9 Hz, C-4), 134.36 (br d, ^1J = 8–10 Hz, C_q-3a), 143.25 (d, ^2J = 4.0 Hz, C_q-7a), 162.00 (d, ^1J = 39.8 Hz, CH-2). ^{31}P NMR ($CDCl_3$): δ = 61.0 (br).

Preparation of Crystals of 5a 2MeOH. Filtration of the suspension formed from **1** (97 mg, 0.47 mmol) and CuCl (140 mg, 1.41 mmol) in THF after 1 day and removal of the solvent from the filtrate gave a yellow viscous residue (ca. 170 mg). The ^{1}H and ^{13}C NMR data in CD_3OD (see Table S2) are similar to those of the above precursor of **2a**·4 THF in CD_3OD; ^{31}P{^{1}H} NMR (CD_3OD): δ = 55.9 (vbr). Slow diffusion of overlayered hexane into a concentrated solution of the residue in THF led to small needle-like crystals,

DOI: 10.1021/ic502367d
Inorg. Chem. 2015, 54, 2117–2127

Table 2. Crystal Data and Structure Refinement for 2a·4THF, 3b, 4b, 4b′, 5a·2MeOH, and 5b·2MeOH

compound	2a·4THF	3b	4b	4b′	5a·2MeOH	5b·2MeOH
empirical formula	$C_{88}H_{128}Cl_9Cu_9N_6O_4P_6$	$C_{48}H_{64}Br_2Cu_2N_4P_4$	$C_{48}H_{64}Br_2Cu_2N_4P_4$	$C_{48}H_{64}Br_2Cu_2N_4P_4$	$C_{50}H_{72}Cl_2Cu_2N_4O_2P_4$	$C_{50}H_{72}Br_2Cu_2N_4O_2P_4$
fw	2410.68	1107.82	1107.82	1107.82	1082.98	1171.90
temp	170(2) K	100(2) K	100(2) K	293(2) K	100(2) K	100(2) K
wavelength	0.71073 Å	1.54184 Å	1.54184 Å	0.71073 Å	0.71073 Å	0.71073 Å
cryst syst	triclinic	triclinic	monoclinic	monoclinic	monoclinic	monoclinic
space group	$P\bar{1}$	$P\bar{1}$	$P2_1/n$	$P2_1/c$	$P2_1/c$	$P2_1/c$
unit cell dimensions	a = 13.330(3) Å, α = 85.18(3)°	a = 8.8940(6) Å, α = 105.610(6)°	a = 23.865(2) Å, α = 90°	a = 11.990(2) Å, α = 90°	a = 12.4305(4) Å, α = 90°	a = 12.4268(3) Å, α = 90°
	b = 13.856(3) Å, β = 81.25(3)°	b = 9.8683(7) Å, β = 105.449(6)°	b = 10.2691(5) Å, β = 101.576(7)°	b = 10.349(2) Å, β = 101.49(3)°	b = 9.9886(3) Å, β = 101.264(4)°	b = 10.0538(2) Å, β = 103.166(3)°
	c = 13.861 (3) Å, γ = 82.12(3)°	c = 15.2708(9) Å, γ = 92.851(6)°	c = 20.6952(15) Å, γ = 90°	c = 20.839(4) Å, γ = 90°	c = 22.9500(7) Å, γ = 90°	c = 23.3797(4) Å, γ = 90°
vol	2501.3(9) Å^3	1233.53(14) Å^3	4968.7(6) Å^3	2533.9(9) Å^3	2794.65(15) Å^3	2844.18(10) Å^3
Z	1	1	4	2	2	2
density (calcd)	1.600 Mg/m^3	1.491 Mg/m^3	1.481 Mg/m^3	1.452 Mg/m^3	1.287 Mg/m^3	1.368 Mg/m^3
abs coeff	2.260 mm^{-1}	4.468 mm^{-1}	4.437 mm^{-1}	2.579 mm^{-1}	1.010 mm^{-1}	2.304 mm^{-1}
F(000)	1234	568	2272	1136	1136	1208
cryst size	0.214 × 0.055 × 0.038 mm^3	0.17 × 0.17 × 0.03 mm^3	0.08 × 0.03 × 0.01 mm^3	0.221 × 0.117 × 0.060 mm^3	0.30 × 0.08 × 0.04 mm^3	0.25 × 0.25 × 0.15 mm^3
ϑ range for data collection	3.240 to 29.317°	4.69 to 75.97°	3.78 to 76.48°	3.468 to 29.252°	2.21 to 30.03°	2.21 to 30.03°
index ranges	$-18 \le h \le 18$, $-18 \le k \le 19$, $-19 \le l \le 16$	$-10 \le h \le 11$, $-12 \le k \le 12$, $-19 \le l \le 19$	$-29 \le h \le 29$, $-12 \le k \le 12$, $-26 \le l \le 25$	$-14 \le h \le 16$, $-14 \le k \le 14$, $-28 \le l \le 28$	$-17 \le h \le 17$, $-14 \le k \le 13$, $-32 \le l \le 32$	$-17 \le h \le 17$, $-14 \le k \le 14$, $-32 \le l \le 32$
reflns collected	27 931	43 349	80 064	27 524	89 129	111 700
independent reflns	13 416 [R(int) = 0.1747]	5102 [R(int) = 0.0372]	10 263 [R(int) = 0.1126]	6838 [R(int) = 0.0961]	8071 [R(int) = 0.0621]	8276 [R(int) = 0.0373]
completeness	99.7% to ϑ = 25.000°	99.6% to ϑ = 75.00°	98.5% to ϑ = 76.48°	99.8% to ϑ = 25.000°	98.8% to ϑ = 30.03°	99.4% to ϑ = 30.03°
abs correction	numerical	semiempirical from equivalents	semiempirical from equivalents	numerical	semiempirical from equivalents	semiempirical from equivalents
max and min transmission	0.9506 and 0.7042	1.00000 and 0.51548	1.00000 and 0.18409	0.9614 and 0.8340	1.00000 and 0.97770	1.00000 and 0.86413
refinement method	full-matrix least-squares on F^2	full-matrix least-squares on F^2	full-matrix least-squares on F^2	full-matrix least-squares on F^2	full-matrix least-squares on F^2	full-matrix least-squares on F^2
data/restraints/params	13416 /15/574	5102/0/277	10263/0/553	6838 /0/277	8071/0/300	8276/0/300
goodness-of-fit on F^2	0.902	1.066	1.016	0.934	1.049	1.068
final R indices [$I > 2\sigma(I)$]	R1 = 0.0997, wR2 = 0.1700	R1 = 0.0291, wR2 = 0.0759	R1 = 0.0466, wR2 = 0.0938	R1 = 0.0406, wR2 = 0.0745	R1 = 0.0337, wR2 = 0.0675	R1 = 0.0278, wR2 = 0.0615
R indices (all data)	R1 = 0.2505, wR2 = 0.2157	R1 = 0.0309, wR2 = 0.0775	R1 = 0.0747, wR2 = 0.1061	R1 = 0.1310, wR2 = 0.1031	R1 = 0.0494, wR2 = 0.0727	R1 = 0.0353, wR2 = 0.0642
largest diff. peak and hole	1.071 and −0.670 e·Å^{-3}	0.685 and −0.542 e·Å^{-3}	0.608 and −0.692 e·Å^{-3}	0.435 and −0.919 e·Å^{-3}	0.563 and −0.373 e·Å^{-3}	0.846 and −0.411 e·Å^{-3}

DOI: 10.1021/ic502367d
Inorg. Chem. 2015, 54, 2117−2127

allowing crystal structure determination. Selected bond lengths and angles are compiled in Table 1, crystal data in Table 2.

Preparation of Crystals *of* 5b·2MeOH. Tetrahydrofuran (10 mL) was added to a mixture of **1** (88 mg, 0.43 mmol) and CuBr·SMe_2 (88 mg, 0.43 mmol) and stirred for 1 d at 20 °C. The insoluble part of the yellow suspension was filtered off and washed with THF. Removal of the solvent from the filtrate gave 180 mg of a yellow viscous residue. ^{1}H NMR (CD_3OD): δ = 0.90 (s, 9 H, CMe_3), 4.08 (s, 2 H, NCH_2), 7.11 (tdd, ^3J = 7.9, 7.2, $^4J_{PH}$ = 1.2, ^4J = 0.6 Hz, 1 H, H-5), 7.38 (br t, ^3J = 8.3, 7.2 Hz, 1 H, H-6), 7.72 (d, ^3J = 8.3 Hz, 1 H, H-7), 7.93 (dd, ^3J = 7.9, $^3J_{PH}$ = 4.5 Hz, 1 H, H-4), 8.46 (d, $^2J_{PH}$ = 35.9 Hz, 1 H, H-2). ^{13}C{^{1}H} NMR (CD_3OD): δ = 28.57 (s, CH_3), 35.36 (s, CMe_3), 61.64 (s, NCH_2), 115.46 (s, C-7), 121.59 (d, ^3J = 11.9 Hz, C-5), 125.96 (s, C-6), 129.93 (d, ^2J = 18.6 Hz, C-4), 144.93 (d, ^2J = 4 Hz, C_q-7a), 163.48 (d, ^1J = 30.5 Hz, CH-2); C_q-3a at noise level. ^{31}P{^{1}H} NMR (CD_3OD): δ = 44 (vbr). HRMS (ESI in MeOH): formula unit $C_{24}H_{32}BrCuN_2P_2$ (553.92), calcd for L_2Cu^+ $[C_{24}H_{32}Cu_1N_2P_2]^+$, 473.1332; found, 473.1344 (100%) and correct isotopic pattern. Crystals of **5b**·2MeOH (ca. 60 mg, 50%) were formed after concentration of a solution of the viscous product in methanol/hexane and addition of a few drops of THF. Selected bond lengths and angles are compiled in Table 1, crystal data in Table 2.

Crystal Structure Analyses. Crystals of **2a**·4THF, **3b**, **4b**, **5a**·2MeOH and **5b**·2MeOH were mounted on glass fibres in inert oil. Diffraction data for a crystal of **2a**·4THF and of **4b** were recorded at −103 and 20 °C, respectively, using a STOE-IPDS 2T diffractometer with graphite-monochromated Mo Kα radiation. The structures were solved by direct methods (SHELXS-97) and refined by full-matrix least-squares techniques (SHELXL-97).[27] All non-hydrogen-atoms were refined with anisotropic displacement parameters. Hydrogen atoms were refined isotropically on calculated positions using riding models with their U_{iso} values constrained to 1.5 U_{eq} of their pivot atoms for terminal sp^3 carbon atoms and 1.2 times for all other carbon atoms. Methyls were refined as idealized rigid groups with their torsion angles taken from electron density (HFIX 137). The unit cell of **2a**·4THF contains four molecules THF per formula; two coordinated to Cu atoms and two as solvent molecules. One of the THF solvents is disordered. The respective carbon−carbon distances were constrained using SADI. Of the four independent Cu atoms in the structure, the one coordinated by THF is disordered over two positions, one position closer to THF, the other closer to the central chloride atom. The crystal of **4b**′ did not display disorders. Data of **3b**, **4b**, **5a**·2 MeOH and **5b**·2 MeOH were recorded at 100 K on Oxford Diffraction diffractometers using monochromated Mo Kα or mirror-focused Cu Kα radiation. *Crystal data* are summarized in Table 2. The structures were refined by full-matrix least-squares on F^2.[27] Hydrogen atoms were freely refined (OH groups), included as part of rigid idealized methyl groups allowed to rotate but not tip, or introduced at calculated positions and refined using a riding model. *Special features*: Structure **4b** has translational pseudosymmetry that mimics a halving of the *a* axis; for the room temperature structure of the same compound **4b**′ the simple subcell (halved in volume compared to **4b**) without this pseudosymmetry was found. **5a**·2MeOH and **5b**·2MeOH are isotypic.

Density functional calculations were carried out by the Gaussian 09 suite of programs.[28] The structure of monomer complexes and of the dimers **3b** and **4b** was optimized at the ωB97xD/cc-PVDZ levels of theory. The AIM analysis was carried out for the ωB97xD/6−31G* electron density of **4b** at the crystal structure geometry.[29]

■ ASSOCIATED CONTENT

Supporting Information

X-ray crystallographic data in CIF format of **2a**·4THF (CCDC 1026420), **4b**′ (CCDC 1040644) and **3b**, **4b**, **5a**·2MeOH and **5b**·2MeOH (CCDC 997386-997389), Tables S1 and S2 with experimental data for conversion of **1** with CuCl and with CuBr in 1:1, 1:2, and 1:3 molar ratios and NMR data of the products, Figures S1−S8 of NMR spectra of THF solvates of **2a** and **2b** and VT NMR spectra of labile complexes, prepared from **1** and CuBr (1:1) in CD_2Cl_2, Figure S9 of the molecular structure of **4b**′ in the crystal, Figures S10−S14 and data of calculated (ωB97xD/cc-PVDZ) optimized geometries of model compounds. This material is available free of charge via the Internet at http://pubs.acs.org.

■ AUTHOR INFORMATION

Corresponding Author

*E-mail: heinicke@uni-greifswald.de. Tel: +49 3834 864318.
*E-mail: nyulaszi@mail.bme.hu. Phone: (+36)14633281(L.N.).

Present Address

$^{\perp}$(M.G.) Chemistry Department, University of Hodeidah, Hodeidah, Yemen.

Notes

The authors declare no competing financial interest.

■ ACKNOWLEDGMENTS

Funding of these studies and a 6-month scholarship (to M.G.) by the *Deutsche Forschungsgemeinschaft* (HE 1997/14-1) and OTKA K 105417 as well as COST CM 1302 is gratefully acknowledged. We thank G. Thede, M. Steinich, and Dr. M. K. Kindermann for NMR and LRMS, Dr. H. Frauendorf and G. Sommer-Udvarnoki (Georg-August-Universität Göttingen, Institut für Organische und Biomolekulare Chemie) for HRMS measurements.

■ REFERENCES

(1) (a) Gusev, D. G. *Organometallics* **2009**, *28*, 763−770. (b) Poë, A. J. *Dalton Trans.* **2009**, 1999−2003. (c) Clarke, M. L.; Frew, J. J. R. *Organometallic Chemistry* **2009**, *35*, 19−46. (d) Kühl, O. *Coord. Chem. Rev.* **2005**, *249*, 693−704. (e) Tolman, C. A. *Chem. Rev.* **1977**, *77*, 313−348.

(2) (a) Behr, A.; Neubert, P. *Applied Homogenous Catalysis*; Wiley-VCH: Weinheim, 2012; Chapter 7. (b) Kollar, L.; Keglevich, G. *Chem. Rev.* **2010**, *110*, 4257−4302. (c) *Phosphorus Ligands in Asymmetric Catalysis*; Börner, A., Ed.; Wiley-VCH: Weinheim, 2008. (d) van Leeuwen, P. W. N. M. *Homogeneous Catalysis: Understanding the Art*, Kluwer Academic Publishers: Dordrecht, 2004. (e) Beller, M.; Bolm, C. *Transition Metals for Organic Synthesis*; Wiley-VCH: Weinheim, 2004.

(3) (a) Müller, C.; Broeckx, L. E. E.; de Krom, I.; Weemers, J. J. M. *Eur. J. Inorg. Chem.* **2013**, 187−202. (b) Müller, C.; Vogt, D. *Dalton Trans.* **2007**, 5505−5523. (c) Le Floch, P. *Coord. Chem. Rev.* **2006**, *250*, 627−681. (d) Breit, B.; Winde, R.; Mackewitz, T.; Paciello, R.; Harms, K. *Chem. Eur. J.* **2001**, *7*, 3106−3121.

(4) (a) Ito, S.; Nishide, K.; Yoshifuji, M. *Organometallics* **2006**, *25*, 1424−1430. (b) Freytag, M.; Ito, S.; Yoshifuji, M. *Chem. Asian J.* **2006**, *1*, 693−700. (c) Weber, L. *Angew. Chem., Int. Ed.* **2002**, *41*, 563−572.

(5) (a) Bansal, R. K. Anellated Azaphospholes. In *Topics in Heterocyclic Chemistry*; Bansal, R. K., Ed.; Springer: Berlin, 2010; Vol. *20*, pp. 1−30. (b) Bansal, R. K.; Heinicke, J. *Chem. Rev.* **2001**, *101*, 3549−3578. (c) Schmidpeter, A. In *Phosphorus-Carbon Heterocyclic Chemistry: The Rise of a New Domain*; Mathey, F., Ed.; Pergamon: Amsterdam, 2001; pp. 363−461.

(6) Recent examples: (a) Ghalib, M.; Niaz, B.; Jones, P. G.; Heinicke, J. W. *Tetrahedron Lett.* **2012**, *53*, 5012−5014. (b) Adam, M. S. S.; Jones, P. G.; Heinicke, J. W. *Eur. J. Inorg. Chem.* **2010**, 3307−3316. (c) Heinicke, J.; Steinhauser, K.; Peulecke, N.; Spannenberg, A.; Mayer, P.; Karaghiosoff, K. *Organometallics* **2002**, *21*, 912−919.

(7) (a) Dash, K. C.; Schmidbaur, H.; Schmidpeter, A. *Inorg. Chim. Acta* **1980**, *41*, 167−170. (b) Kraaijkamp, J. G.; Grove, D. M.; van Koten, G.; Schmidpeter, A. *Inorg. Chem.* **1988**, *27*, 2612−2617. (c) Weber, L.; Kaminski, O.; Stammler, H. G.; Neumann, B. *Organometallics* **1995**, *14*, 581−583. (d) Sklorz, J. A. W.; Hoof, S.;

DOI: 10.1021/ic502367d
Inorg. Chem. 2015, 54, 2117−2127

Sommer, M. G.; Weißer, F.; Weber, M.; Wiecko, J.; Sarkar, B.; Müller, C. *Organometallics* **2014**, *33*, 511−516.
(8) Kornev, A. N.; Sushev, V. V.; Panova, Y. S.; Lukoyanova, O. V.; Ketkov, S. Y.; Baranov, E. V.; Fukin, G. K.; Lopatin, M. A.; Budnikova, Y. G.; Abakumov, G. A. *Inorg. Chem.* **2014**, *53*, 3243−3252.
(9) Angermund, K.; Eckerle, A.; Monkiewicz, J.; Krüger, C.; Wilke, G. *Inorg. Chim. Acta* **1998**, *270*, 273−278.
(10) (a) Ghalib, M.; Könczöl, L.; Nyulászi, L.; Jones, P. G.; Palm, G. J.; Heinicke, J. W. *Dalton Trans.* **2014**, *43*, 51−54. (b) Ghalib, M.; Könczöl, L.; Nyulászi, L.; Palm, G. J.; Schulzke, C.; Heinicke, J. W. *Dalton Trans.* **2015**, *44*, 1769−1774.
(11) Aluri, B. R.; Kindermann, M. K.; Jones, P. G.; Dix, I.; Heinicke, J. W. *Inorg. Chem.* **2008**, *47*, 6900−6912.
(12) Lenders, B.; Grove, D. M.; Smeets, W. J. J.; van der Sluis, P.; Spek, A. L.; van Koten, G. *Organometallics* **1991**, *10*, 786−791.
(13) (a) Nyulászi, L. *Chem. Rev.* **2001**, *101*, 1229−1246. (b) Nyulászi, L.; Csonka, G.; Réffy, J.; Veszprémi, T.; J. Heinicke, J. *J. Organomet. Chem.* **1989**, *373*, 49−56.
(14) (a) Healy, P. C.; McMurtrie, J. C.; Bouzaid, J. *Acta Crystallogr., Sect. E: Struct. Rep. Online* **2010**, *66* (Pt 5), m493−m494. (b) Vinogradova, K. A.; Krivopalov, V. P.; Nikolaenkova, E. B.; Pervukhina, N. V.; Naumov, D. Y.; Rakhmanova, M. I.; Boguslavsky, E. G.; Sheludyakova, L. A.; Bushuev, M. B. *Polyhedron* **2013**, *57*, 1−13. (c) Rodenstein, A.; Creutzburg, D.; Schmiedel, P.; Griebel, J.; Hennig, L.; Kirmse, R. *Z. Anorg. Allg. Chem.* **2008**, *634*, 2811−2818. (d) Mirkhani, V.; Harkema, S.; Kia, R. *Acta Crystallogr., Sect. C: Struct. Chem.* **2004**, *60*, m343−m344. (e) Healy, P.; Kildea, J.; Skelton, B.; White, A. *Aust. J. Chem.* **1989**, *42*, 115−136. (f) Meng, Q.; Chen, Y.; Li, B.; Chen, S.; Gao, S. *Acta Crystallogr., Sect. E: Struct. Rep. Online* **2011**, *67*, m226.
(15) Engberg, A. *Acta Chem. Scand.* **1970**, *24*, 3510−3526.
(16) Hargittai, M.; Schwerdtfeger, P.; Reffy, B.; Brown, R. *Chem. Eur. J.* **2003**, *9*, 327−333.
(17) (a) Le Floch, P.; Richard, L.; Mathey, F. *Bull. Soc. Chim. Fr.* **1996**, *133*, 691−696. (b) Mézailles, N.; Le Floch, P.; Waschbüsch, K.; Ricard, L.; Mathey, F.; Kubiak, C. P. *J. Organomet. Chem.* **1997**, *541*, 277−283. (c) Moores, A.; Mézailles, N.; Maigrot, N.; Ricard, L.; Mathey, F.; Le Floch, P. *Eur. J. Inorg. Chem.* **2002**, 2034−2039. (d) Shiotsuka, M.; Tanamachi, T.; Urakawa, T.; Munakata, M.; Matsuda, Y. *J. Supramol. Chem.* **2002**, *2*, 211−217. (e) Roesch, P.; Nitsch, J.; Lutz, M.; Wiecko, J.; Steffen, A.; Müller, C. *Inorg. Chem.* **2014**, *53*, 9855−9859.
(18) Müller, C.; Pidko, E. A.; Lutz, M.; Spek, A. L.; Vogt, D. *Chem. Eur. J.* **2008**, *14*, 8803−8807.
(19) Mao, Y.; Lim, K. M. H.; Li, Y.; Ganguly, R.; Mathey, F. *Organometallics* **2013**, *32*, 3562−3565.
(20) (a) Gudat, D.; Schrott, M.; Nieger, M. *J. Chem. Soc., Chem. Commun.* **1995**, 1541−1542. (b) Gudat, D.; Holderberg, A. W.; Korber, N.; Nieger, M.; Schrott, M. *Z. Naturforsch.* **1999**, *54b*, 1244−1252.
(21) (a) Nobel, D.; van Koten, G.; Spek, A. L. *Angew. Chem., Int. Ed. Engl.* **1989**, *28*, 208−210. (b) van Koten, G. *J. Organomet. Chem.* **1990**, *400*, 283−301 and references therein.
(22) Heinicke, J.; Gupta, N.; Singh, S.; Surana, A.; Kühl, O.; Bansal, R. K.; Karaghiosoff, K.; Vogt, M. *Z. Anorg. Allg. Chem.* **2002**, *628*, 2869−2876.
(23) Schleyer, P. v. R.; Maerker, C.; Dransfeld, A.; Jiao, H.; van Eikema Hommes, N. J. R. *J. Am. Chem. Soc.* **1996**, *118*, 6317−6318.
(24) Bader, R. F. W. *Atoms in Molecules: A Quantum Theory*; Oxford University Press: Oxford, 1990. (b) Bader, R. F. W. *Acc. Chem. Res.* **1985**, *18*, 9−15.
(25) Dinda, S.; Samuelson, A. G. *Chem. Eur. J.* **2012**, *18*, 3032−3042.
(26) Brauer, G. *Handbuch der Präparativen Anorganischen Chemie, Vol. II*, **1978**, p. 973, p. 974.
(27) Sheldrick, G. M. *SHELXL-97*; University of Göttingen, Göttingen, Germany.
(28) Frisch, M. J.; Trucks, G. W.; Schlegel, H. B.; Scuseria, G. E.; Robb, M. A.; Cheeseman, J. R.; Scalmani, G.; Barone, V.; Mennucci, B.; Petersson, G. A.; Nakatsuji, H.; Caricato, M.; Li, X.; Hratchian, H. P.; Izmaylov, A. F.; Bloino, J.; Zheng, G.; Sonnenberg, J. L.; Hada, M.; Ehara, M.; Toyota, K.; Fukuda, R.; Hasegawa, J.; Ishida, M.; Nakajima, T.; Honda, Y.; Kitao, O.; Nakai, H.; Vreven, T.; Montgomery, J. A., Jr.; Peralta, J. E.; Ogliaro, F.; Bearpark, M.; Heyd, J. J.; Brothers, E.; Kudin, K. N.; Staroverov, V. N.; Kobayashi, R.; Normand, J.; Raghavachari, K.; Rendell, A.; Burant, J. C.; Iyengar, S. S.; Tomasi, J.; Cossi, M.; Rega, N.; Millam, J. M.; Klene, M.; Knox, J. E.; Cross, J. B.; Bakken, V.; Adamo, C.; Jaramillo, J.; Gomperts, R.; Stratmann, R. E.; Yazyev, O.; Austin, A. J.; Cammi, R.; Pomelli, C.; Ochterski, J. W.; Martin, R. L.; Morokuma, K.; Zakrzewski, V. G.; Voth, G. A.; Salvador, P.; Dannenberg, J. J.; Dapprich, S.; Daniels, A. D.; Farkas, O.; Foresman, J. B.; Ortiz, J. V.; Cioslowski, J.; Fox, D. J. *Gaussian 09*, revision B.01; Gaussian, Inc.: Wallingford, CT, 2010.
(29) Keith, T. A. *AIMAll*, version 11.10.16; Gristmill Software: Overland Park, KS, 2011. http://aim.tkgristmill.com.

DOI: 10.1021/ic502367d
Inorg. Chem. 2015, 54, 2117−2127